Multipactor Prediction for On-Board Spacecraft RF Equipment With the MEST Software Tool

Juan de Lara, Francisco Pérez, Manuel Alfonseca, Luis Galán, Isabel Montero, Elisa Román, and David Raboso Garcia-Baquero

Abstract—**Within the framework of a project sponsored by the European Space Agency (ESA), we have developed a software tool to predict the occurrence of multipactor discharge in a simple radio frequency (RF) device modeled as parallel plates. The tool uses a micro-level explicit representation of the electrons (i.e., each electron in the system is modeled separately), and includes a detailed Monte Carlo model of the secondary electron emission process in the plates. Materials secondary emission yield (SEY) is described using either the usual parameter set (E_1, E_2, and σ_{max}), or a more detailed model, where the contributions due to true secondary, backscattered or elastically reflected electrons are given their own sets of parameters, together with additional parameters for the angle dependence. The simulator has been validated using experimental data gathered at ESA and the Universidad Autónoma de Madrid, Madrid, Spain. The simulator helped in the selection of material coatings for the mitigation of Multipactor effect in RF transmission lines on-board satellite payloads.**

Index Terms—**Multipactor simulation, secondary emission simulation, simulation software.**

I. INTRODUCTION

THE MULTIPACTOR effect [1], [2] is a spurious discharge that may take effect in a waveguide as a consequence of the electron avalanche produced when the secondary electrons, ripped away from the inner walls of the waveguide by the impact of free electrons, resonate with the electric field transmitted by the waveguide. The discharge produced, as a consequence of the continual increase of the number of electrons in the vacuum filling the waveguide, makes this unusable and is an important danger to be avoided.

To avoid multipactor, different material coatings have been tested with the aim of reducing the secondary emission of the walls. The effect is prone to appear in the sections where the waveguide caliber is smallest, as in the different filters located inside the waveguide to control its impedance and its frequency
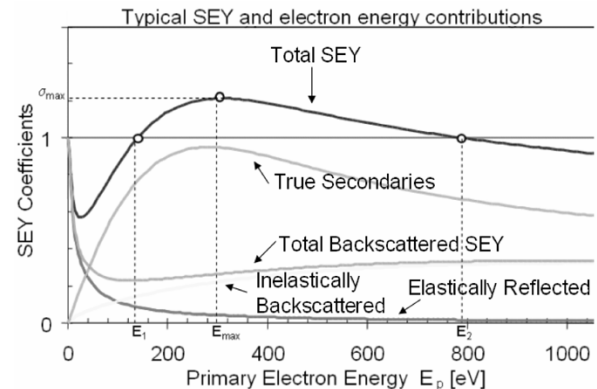
Fig. 1. Typical SEY and different kinds of emission contributions.

response properties. Multipactor experiments are relatively expensive, time and resource consuming. Thus, with appropriate models of the phenomena and if the different materials can be characterized, simulation can be a valuable tool for selecting the most promising materials.

With this aim, we have developed the software tool MEST (multipactor electron simulation tool). The system performs simulations where each electron is individually tracked. We follow a discrete-event approach [3], where the events are the collisions of electrons with the waveguide walls. The impacting electron can be absorbed, elastically or inelastically reflected, or true secondaries can be produced. In the latter case, the generated electrons are incorporated to the simulation and individually tracked in their turn. Materials are described either using the usual parameter set (E_1, E_2, and σ_{max}, see Fig. 1), or by a more detailed model, where the contributions due to true secondary, backscattered or elastically reflected electrons are given their own sets of parameters, together with additional parameters for the angle dependence. The simulator generates V–$f \cdot d$ maps of the multipactor discharge detected in the simulations and other graphical outputs that help understanding the experiment.

The rest of the paper is organized as follows. In Section II, we briefly explain the models and assumptions used in the software. Section III describes the MEST software. Section IV describes obtained results for some materials. Finally, Section V ends with the conclusion and the future work.

II. MODELS USED IN THE SOFTWARE

Models are mathematical descriptions of a certain system that introduce simplifications. These are made in order to make the experimentation with the model (its simulation) more effective

by suppressing intricacy not affecting significantly the results, or because the exact characterization of the phenomena is not known or cannot be made. Nonetheless, the use of simulation is preferred in those applications where direct experimentation is expensive, dangerous, or nonethical.

In our system, we have considered infinite and finite parallel plates in the xy plane, with the RF electric field unidirectional in the z coordinate. Thus, border effects are not considered, apart from simple termination of the field and electron trajectories in the case of finite size. The approximation corresponds to a narrow gap relative to the other dimensions. This is a good model for a waveguide in which the xy plate is ten or more times bigger than the z gap.

The main characteristic of the software is that electron trajectories are individually modeled and tracked. This is a major difference with most existing simulation software [4]–[7], where packets (also called super-particles) containing a number of electrons (even fractions of them) are considered, all with the same dynamical variables. The number of electrons and the packet variables change each time the packet collides with one of the walls. In models of this kind, the statistical representation of the process becomes progressively worse as the number of electrons increase while the number of packets remain constant or decrease slowly (by absorption). In particular, in particle-in-cell simulators (PIC) [8], the geometry is discretized as cells, in order to calculate the electromagnetic field. Cells contain super-particles, which are moved simultaneously with the same time increment. In our case, such space discretization is not needed, as the geometry we use permits analytically solving the field equations, which is more efficient than the PIC approach for this particular geometry.

In addition, we assume that electron trajectories are only modified by the electromagnetic field and are not affected by other electrons in the system. That is, effects due to space charge are not taken into account, nor are loading or detuning effects considered. This is correct if only the onset of the multipactor discharge is to be detected. Note, however, that PIC codes usually take these effects into account.

The collision of an electron with a plate can rip zero (absorption) or more electrons from the wall with a probability described below. The newly created electrons are again individually tracked. Given the parameters of a certain material, the SEY depends only on the primary energy E_p and the incidence angle φ of the impacting electron. Following the energy conservation principle, the total kinetic energy of all the output electrons should be equal or less than the input electron kinetic energy. For the initial conditions, a certain number of free electrons (uniformly created during the first period of the electromagnetic field) are assigned a normally distributed energy and angle and start at one of the plates.

When an electron collides with one of the plates, it can be absorbed, elastically or inelastically backscattered, or a number of true secondary electrons may be generated. The three kinds of emitted electrons provide their own contributions to the SEY curve, which is represented as a function of the impacting energy and the incidence electron angle. The addition of the three contributions results in the total SEY. Fig. 1 shows a typical SEY curve for a given angle. In this figure, E_1 and E_2 are defined as

the energy of the first and second intersection of the SEY with a value of 1. $E_{\max}$ is the energy at which the SEY reaches its maximum value ($\sigma_{\max}$).

We have modeled the contribution of inelastically backscattered electrons by

$$
\eta(E_p) = a \cdot (1 - b \cdot E_p) \cdot E_p^{\gamma} \cdot \exp\left(-\left(\frac{E_p}{E_b}\right)^{\mu}\right);
$$
$$
E_b = c + d \cdot Z \tag{1}
$$

where Ep is the primary electron energy $[eV] \leq 5000$ eV, Z is the atomic number of the coating material, a is a property of the material, usually in the range $[7 \times 10^{-3}, 10 \times 10^{-3}]$, $b = 3.0 \times 10^{-5}$, $c = 300$, $d = 175$, $\gamma = 0.56$, $\mu = 0.70$.

The contribution from elastically backscattered electrons is given by

$$
\varepsilon(E_p) = \frac{\varepsilon_1}{1 + \frac{E_p}{E_{e_1}}} + \frac{\varepsilon_2}{1 + \frac{E_p}{E_{e_2}}} \tag{2}
$$

where $\varepsilon_1 = \varepsilon_o - \varepsilon_2$, ε_o is the value of the elastic contribution for $E_p = 0$, usually 1 [9], $\varepsilon_2 = 0.07$, $E_{e1} = g/\sqrt{Z}$, $E_{e2} = h \cdot Z^2$, $g = 50$, $h = 0.25$.

Finally, the contribution due to true secondary electrons is

$$
\delta(E_p) = \delta_m \cdot \frac{s \cdot \frac{E_p}{E_m}}{s - 1 + \left(\frac{E_p}{E_m}\right)^s} \tag{3}
$$

where δ_m, E_m, and s are parameters of the material.

Additionally, the last three expressions have to take into account the angle φ (respect to the inward normal to the xy plane) with which the electron collides. This can be modeled as follows:

$$
\delta(E_p, \varphi) = \delta(E_p) \frac{k + 1}{k + \cos(\varphi)} \tag{4}
$$

where $k = p \cdot Z + r$, $p = 0.0027$.

$$
\eta(E_p, \varphi) = \eta(E_p)^{\cos(\varphi)} \cdot C_1^{1 - \cos(\varphi)}
$$
$$
C_1 = \chi \cdot \frac{\eta(E_p)}{\eta(E_p) + \varepsilon(E_p)} \tag{5}
$$
$$
\varepsilon(E_p, \varphi) = \varepsilon(E_p)^{\cos(\varphi)} \cdot C_2^{1 - \cos(\varphi)}
$$
$$
C_2 = \chi \cdot \frac{\varepsilon(E_p)}{\eta(E_p) + \varepsilon(E_p)} \tag{6}
$$

where $\chi = 0.89$, and note that $C_1 + C_2 = \chi$.

For a clean flat surface, $r = 0$. For rough surfaces, $2.5 < r < 10$; typically, $r = 5$.

These models result from fitting experimental data for many materials, either from our own experimental data or from the literature, mostly from [10].

When an electron impacts a plate, the probability for each kind of emission is thus given by

$$
P_e(E_p, \varphi) = \varepsilon(E_p, \varphi)
$$
$$
P_b(E_p, \varphi) = \eta(E_p, \varphi)
$$
$$
P_s(E_p, \varphi) = 1 - P_e(E_p, \varphi) - P_b(E_p, \varphi). \tag{7}
$$

The probabilities of a collision producing elastic or inelastically backscattered electrons are $P_e(E_p, \varphi)$ and $P_b(E_p, \varphi)$, respectively. Both types of collisions produce one emitted electron. In the first case (elastic), the incoming electron is perfectly reflected. In the second case (inelastic), the electron penetrates into the material, one electron scatters from atoms inside the material, and is reflected out with energy loss. These electrons are sometimes called rediffused [11]. In the true secondary emission case, the electrons interact with the material in a more complicated way. This collision has a probability $P_s(E_p, \varphi)$, and a random number of electrons are produced. Their number (in the case of true secondaries) and energies (for both secondaries and inelastic) are calculated, as shown in Section II-A.

A. Calculating the Number of Secondary Electrons in a Collision

In the case of an inelastic backscattering collision, the energy of the emitted electron is calculated by the inverse cumulative probability function

$$G_b(u) = \alpha^{(-1/n_b)} \cdot (\arccos(1 - \beta \cdot u))^{(1/n_b)}$$
$$\beta = 1 - \cos(\alpha) \quad \alpha = \pi \cdot X_{cb}^{n_b} \quad (8)$$

where n_b and X_{cb} are parameters of the material. First, a random number u is generated with uniform probability in $[0, 1]$, and then, the energy of the emitted electron is

$$E_b = E \cdot G_b(u). \quad (9)$$

In the case of a true secondary emission collision, a random number n of secondary electrons are generated with a probability $P_n(Ep, \varphi)$. This probability has a Poisson distribution

$$P_n(E_p, \varphi) = \text{Poisson}_n(\lambda) = \frac{e^{-\lambda} \cdot \lambda^n}{n} \quad (10)$$

where λ is the distribution average. Please note that, while $P_s(E_p, \varphi)$ is the probability that a collision produces true secondary electrons, $P_n(E_p, \varphi)$ is the probability for this collision to produce n electrons. Thus, in order to get the proper average number of true secondary electrons generated per impacting electron (λ)

$$\lambda(E_p, \varphi) = \frac{\delta(E_p, \varphi)}{1 - \varepsilon(E_p, \varphi) - \eta(E_p, \varphi)}. \quad (11)$$

Once the number of true secondary electrons has been obtained, their energy is sequentially computed by the inverse cumulative probability function shown as follows:

$$G_s(u) = \left(\frac{2}{\pi} \cdot \arctan\left(\sqrt{\tan\left(\frac{\pi}{2} \cdot X_{cs}\right) \cdot \tan\left(\frac{\pi}{2} \cdot u\right)}\right)\right)^{(1/n_s)} \quad (12)$$

where n_s is a property of the material, and X_{cs} is calculated as follows:

$$E_{trunc} = \begin{cases} E_{\text{remain}}, & \text{if } (E_{\text{remain}} \geq 1 \text{ eV}) \\ 1, & \text{otherwise} \end{cases}$$
$$X_c = \frac{4 \cdot \left(B - e^{(-E_{trunc}/A)}\right)}{E_{trunc}}$$
$$X_{cs} = \frac{X_c}{(0.9 + 1.1 \cdot X_c)} \quad (13)$$

where A and B are parameters of the material. The energy is calculated for each emitted electron as follows:

$$E_{se} = E_{\text{remain}} \cdot G_s(u) \quad (14)$$

where, for the first of the n secondaries

$$E_{\text{remain}}(\text{first}) = E_p \quad (15)$$

and for the following ones:

$$E_{\text{remain}} = E_{\text{remain}}(\text{previous}) - E_{se}(\text{previous}). \quad (16)$$

Thus, E_{remain} represents the remaining energy to be distributed between the secondary electrons.

We consider emission angles θ, with respect to the inward normal to the xy plane, and ζ in the xy plane. If the output electron is elastically or inelastically backscattered, its output angles are assigned as follows: $\theta = \varphi$ (where θ is the output angle) and $\zeta_{\text{out}} = \zeta_{\text{in}}$.

In the case of a true secondary electron, the angles are calculated using the cosine law distribution as follows:

$$\theta = \arcsin\left(\sqrt{x^2 + y^2}\right); \quad \zeta = \arctan\left(\frac{y}{x}\right) \quad (17)$$

where x and y are random numbers with uniform probability in $[-1, 1]$, such that $x^2 + y^2 \geq 1$. The sign of x and y determines the quadrant of the sphere (always in the inner side of the collision plate): positives x and y correspond to the first quadrant, negative x and positive y to the second, negatives x and y to the third, and positive x and negative y to the fourth quadrant.

B. Simulation Procedure

For the simulation, we have used a typical discrete-event procedure [3]. In this kind of simulation, the time advance is driven by the occurrence of the events (changes in the system state). Thus, the main idea is to have an event queue (also called future event list), ordered by the time of the event. In our case, the events are the impacts of the electrons with the plates. The collision time can be efficiently calculated, because in the case of a parallel plates geometry, we can compute solutions to the electron trajectories analytically. The simulator loops through all the events in the queue, advancing the simulation time, generating new events (new collisions) and placing them in time order in the queue. Therefore, we do not move all the particles simultaneously (as in the PIC codes), but each electron is moved independently to its next collision. The electron state does not need to be calculated or saved in intermediate instants, but only at the collisions. Note, also that having two or more simultaneous events is possible, which will be stored in the order in which they are produced. In fact, they could have been processed in any order, for, in our case, the events already in the queue do not depend on one another.

As stated before, each electron is individually modeled. Following the object-oriented paradigm [12], each electron has been represented as an object, which has the capability to compute the time of its next collision and schedule new collision events for the given time. Thus, each collision event has a link to the electron that generated it.

Conceptually, the simulation procedure follows the control graph shown in Fig. 2. Initially, a population of electrons is generated. Each electron is given a normally distributed energy. All
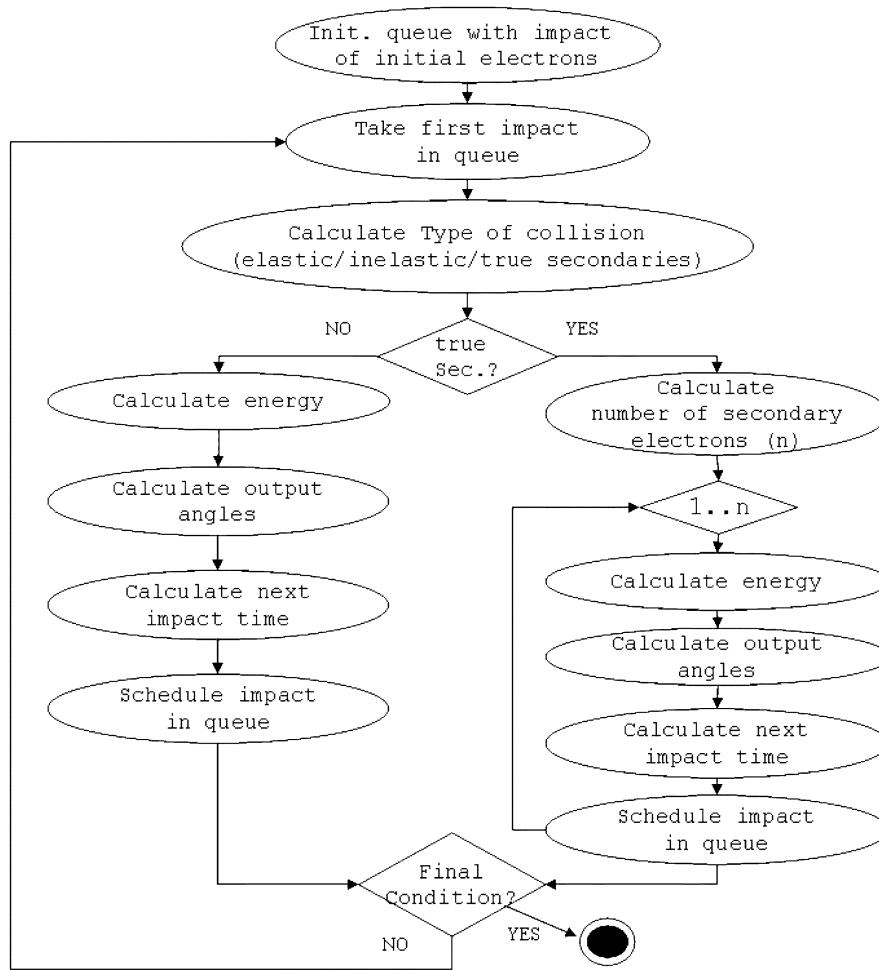
Fig. 2.   Simulation procedure.

start at one of the plates. Moreover, they are assumed to have impacted that plate at a random time in the first period of the electromagnetic field. In this way, this collision initial time is used to initialize the event queue. Then the main simulation loop begins. The simulator takes the first event in the queue, and the associated electron. It calculates the type of collision using the model of the previous section. For each newly generated electron in the collision, it calculates the next impact time and schedules new events. Here, absorption may occur, thus no new event is generated and the electron is deleted from the simulation. The simulation ends when a final condition is met (multipactor appears, does not happen, or a certain number of cycles is reached). The final conditions are discussed in Section II.

III. SOFTWARE

The simulator (MEST) has been implemented in C++ using the Microsoft Foundation Classes and runs in Windows'98 and higher versions. A screenshot of the tool's main window is shown in Fig. 3. The left part of the window is used to enter the initial conditions of the simulation (initial number of electrons, average energy, and dispersion of the initial electrons and their initial angle). It is possible to specify intervals for the gap distance d, and gap voltage V, in such a way that one simulation is performed for each combination of their values. The lower box
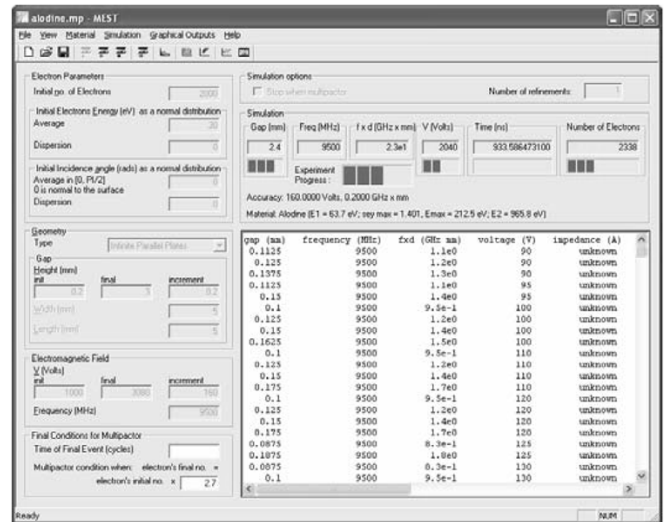

Fig. 3.   MEST main window.

(labeled "Final Conditions") allows the user to specify a final time for the simulation as well as final conditions based on the number of electrons remaining with respect to the initial ones. The latter condition is useful to identify multipactor discharges or situations where all the electrons are absorbed.

The box labeled "Simulation options" to the right allows the user to choose between simulating all the combinations of V, f and d, or looking for the lower and higher values of voltage, gap and frequency which produce multipactor. Thus, only the borders of the multipactor V–$f \cdot d$ region are calculated but not the inner points. It is also possible to choose a number of refinements for higher precision (the step size is halfed progressively) in finding the borders of the curve. These refinements are applied in the $x(f \cdot d)$ and $y(V)$ directions. In the multipactor discharge view (see for example Fig. 9), we use different colors to indicate the probability of multipactor. We calculate a qualitative measure (which we call *susceptibility*), taking into account the rate of change of the number of electrons (positive if they increase) with respect to time. In this way, when multipactor occurs, the quantity is positive (the bigger, the appearance of multipactor is more probable), otherwise it is negative (the bigger in absolute value, the nonappearance of multipactor is more probable). In the graphic, we use orange, orange-red, and red for increasingly probable multipactor, and green, blue-green, blue, and dark blue for decreasingly probable multipactor. Thus, dark-blue corresponds to a negligible probability of multipactor, while red depicts a strong probability of multipactor.

The text boxes inside the panel labeled "Simulation" show the simulation results as they are computed, while the text box at the bottom prints one line with the results for each simulation that produces multipactor. The line shows information about the conditions of the experiment (gap, frequency, voltage, power, initial number of electrons), and the simulation results (phase of first collision, multipactor, final simulation time, final number of electrons, impedance, and susceptibility).

The properties of the material are entered using a separate dialog box. We can use two sets of parameters. The one explained in the previous section, or the more traditional based on E_1, E_2, and $\sigma_{\max}$. Given the values of one of the parameter sets, MEST calculates the values of the other one. The SEY curve for the material can also be visualized, showing the three main components, as Fig. 4 shows.

Once the experiment and the properties of the material have been set, the simulation can start. Several outputs are available during simulation. Figs. 5–7 show the output window which depicts the evolution of the electron population with respect to time. The first two experiments (for Alodine) start with 2000 electrons while the third (for Aluminum) starts with 1000.

In the three cases, there is a transitory period at the beginning of the simulations, where the number of electrons may change erratically. This effect is due to the fact that some initial electrons are not synchronized with the frequency of the RF field, as they are uniformly distributed in the first period of the RF field. In Fig. 5, the number of electrons increases in steps of three RF periods approximately, while in Fig. 6, the population goes down, also with peaks of resonance each three RF periods. This is due to the fact that resonant electrons happen to take about three RF periods to reach the opposite plate in the conditions of the experiment corresponding to Fig. 6. The number of semi-periods taken by an electron to go from one plate to the other is related to the "multipactor mode", see discussion below.

In Figs. 5 and 6, the final condition makes the experiment stop if the number of electrons reaches 2.7 times the initial one
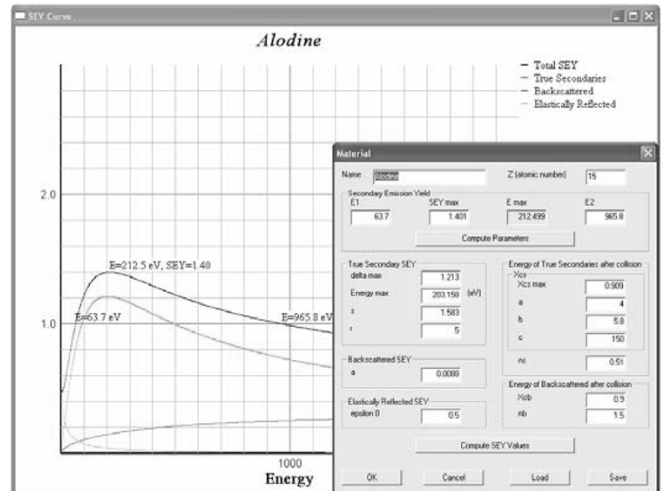

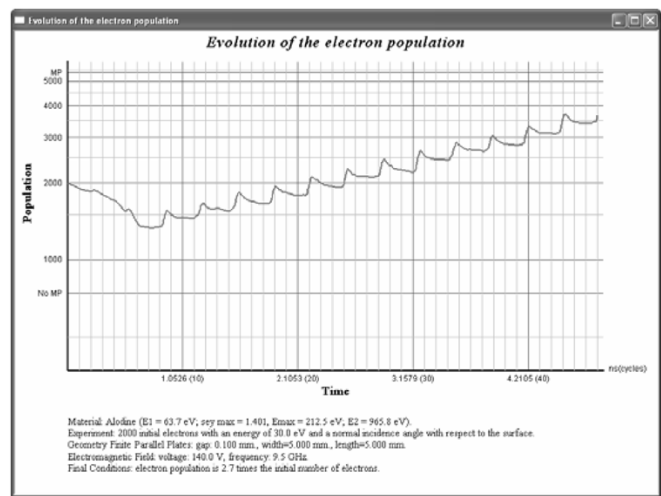Fig. 4.   Defining the parameters for a material with MEST.

Fig. 5.   Evolution of the number of electrons (increasing) in a simulation of Alodine with MEST.
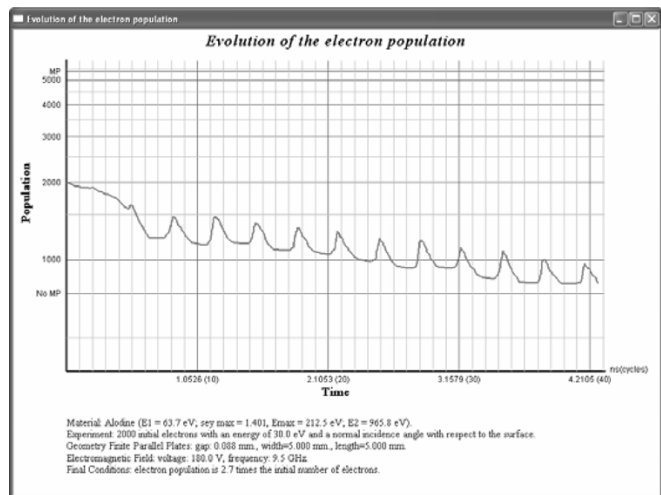

Fig. 6.   Evolution of the number of electrons (decreasing) in a simulation of Alodine with MEST.

number (when the experiment is considered multipactor positive), or 2.7 times less (and the experiment is considered mul-
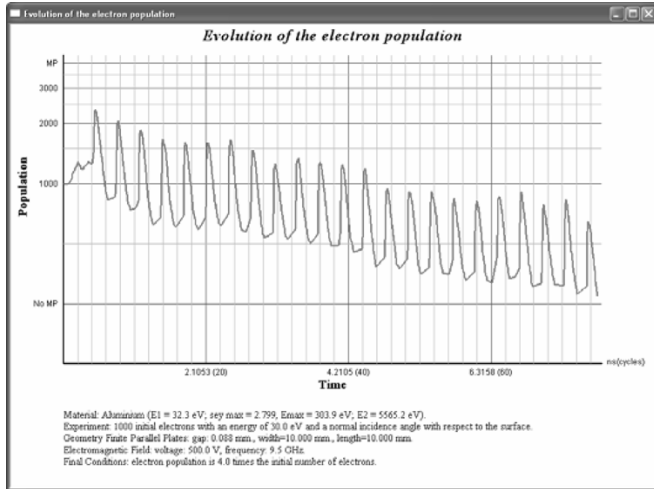
Fig. 7. Evolution of the number of electron in a simulation of Aluminum with MEST.

Fig. 8. Animation of the electron cloud, in a simulation of Alodine.

tipactor negative). For Fig. 7, this final condition is 4 times. The experiment conditions are described at the bottom of each window. In the actual experiments, those in Figs. 6 and 7 resulted multipactor negative, while the one in Fig. 5 came to be multipactor positive.

Thus, the final condition for the simulation can be expressed as a factor of the original number of electrons. It is the responsibility of the experiment designer to assign a meaningful value, but MEST gives a warning if this value is too low. Experimentally, we have found that a factor higher than the maximum SEY ($\sigma_{\max}$) is needed for the final condition, as, in each cycle, the net electron increment is limited by this parameter. Moreover, there are experiments where the number of electrons increases initially, but later decreases until a condition of "no multipactor" appears, as in Fig. 7. Note how the $\sigma_{\max}$ coefficient of this kind of Aluminum is 2.799, thus we may have an increment of 2.799 times the actual number of electrons. Although there are abrupt increments of the number of electrons, the overall tendency is to absorption, as it finally happens. With a lower final condition, such as 2.5 times the number of electrons, we would have incorrectly stopped the experiment signalling a multipactor occurrence. In addition, it can be observed that the peak increments in Figs. 5 and 6 are smaller than the ones of Fig. 7. This is due to the fact that $\sigma_{\max}$ for this kind of Alodine is 1.751 (1.6 times less than its value for Aluminum). In addition, an extra finalization condition can be set when a certain number of cycles are reached.

Fig. 8 shows an additional output window, in which the positions of the electrons can be seen at each instant of time as they move. This animation is shown at run time, while the simulation is being executed. The electron color depicts the number of collisions they have experimented with the walls. In this way, the newly emitted secondary electrons start in black, and as they experiment more collisions, they turn into red. Fig. 8 shows an experiment for Alodine with finite parallel plates, giving the actual electrons positions in space. A similar output window exists for infinite parallel plates. Note that, since our simulator only calculates electron positions at wall collisions, when this window is opened, additional calculations of intermediate positions have to be performed as a function of the actual value of time.
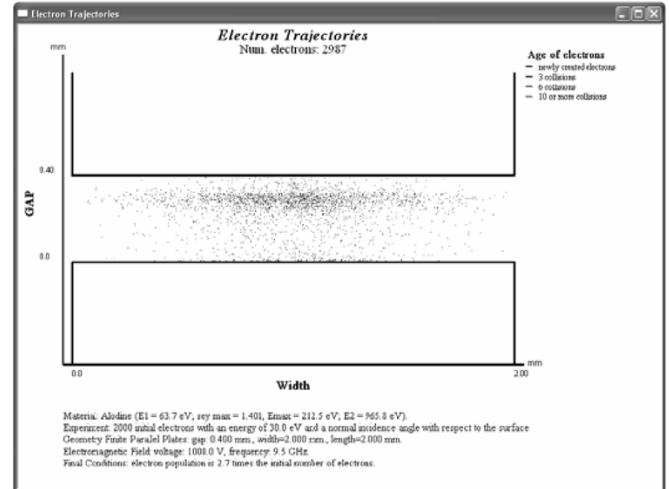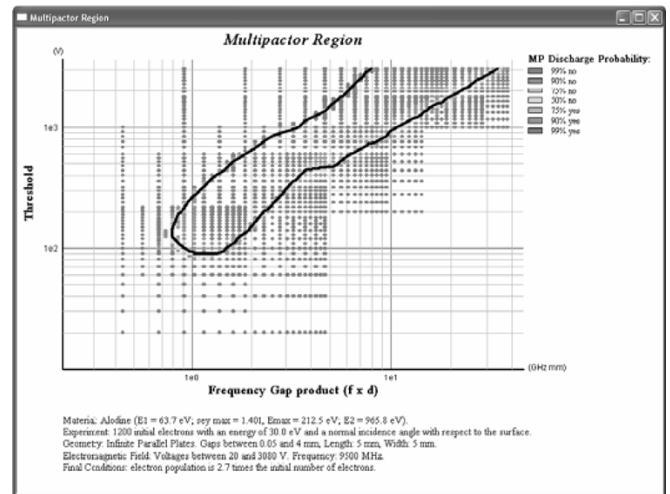

Fig. 9. V–$f \cdot d$ multipactor region for Alodine with MEST.

Fig. 9 shows a graphical output depicting the V–$f \cdot d$ region for Alodine, where each point is one simulation. As stated before, the color of the point depicts the probability of multipactor (the *susceptibility*). Red and orange means multipactor, while blue and green means no multipactor.

Finally, Fig. 10 presents an output window showing the *modes* for the multipactor region in Fig. 9. The modes are defined according to Hatch and Williams [13] as the integer number of RF periods an electron takes to go from one impact to the next one, plus one. Thus, mode 1 is just a semi-period, as it is the minimum time an electron takes to go from one side to the other of the geometry. The figure shows the modes for a simulation with Alodine, in which the first nine modes are shown. Other, higher modes may occur at higher voltages, but the simulation stopped at 3000 V.

IV. VALIDATION AND RESULTS

For a model to be considered correct, validation is necessary. Several kind of validations are possible, among them, structural validation (i.e., checking the correctness of the model description), and a validation of the results.
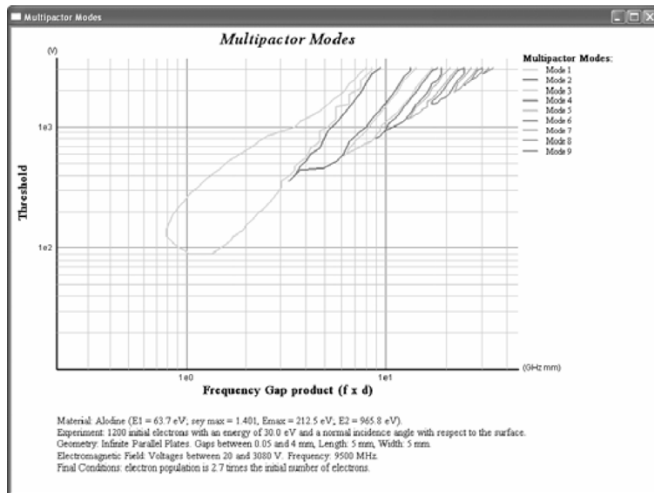
Fig. 10. Multipactor modes for Alodine with MEST.

Fig. 11. Experimental data for Alodine from ESTEC, fitted with Hatch and Williams model, taken from [14].

Fig. 12. $V–f \cdot d$ region for Aluminum with MEST.

Fig. 13. Experimental data for Aluminum from ESTEC, fitted with Hatch and Williams model, taken from [14].

We have validated our software in several steps. First, we validated the distribution of the output angles of secondary electrons (they should follow a cosine law distribution). Then, we calculated the energy spectrum of emitted secondary electrons ($\partial \sigma / \partial E$) for given input values (certain materials and certain electron energy values). They showed good agreement with experimental curves.

We have collected a database of material SEY parameters (obtained from experimental data and the literature). For a particular material, we may have different parameters, depending on the conditions of the measured material (air exposure, deposition technique, etc). Thus, for example, for Alodine we have parameters showing different SEY characteristics ranging from very good secondary emission properties ($E_1 \approx 68$ eV and $\sigma_{max} \approx 1.25$), to very bad ones ($E_1 \approx 30$ eV and $\sigma_{max} \approx 2$) [14]. Note, however, that the overall secondary emission characterization of a material does not only depend on E_1 and σ_{max}, but on the whole parameter set. Thus, it may be possible to have a material with lower σ_{max}, but with worse multipactor characterization (lower voltage of the first positive multipactor experiment). This fact can be possible if the energy E_1 is small, or if the area of the overall SEY curve is bigger.

In the final validation step, we compared the multipactor regions with experimental data obtained from ESTEC [14], also showing good agreement. For example, Fig. 11 shows experimental data from ESTEC (eight experiments, shown with dots) for Alodine [14], fitted with the multipactor model from Hatch and Williams' theory [13]. The material in the database with the more approximate SEY parameters corresponds to the one in Figs. 9 and 10, which show close similarity.

Finally, Figs. 13 and 15 show the theoretical and experimental results for Aluminum and Copper, respectively, which can be compared with the simulation results in Figs. 12 and 14.

For all tested materials, although regions show good agreement with experimental data, note, however, that Hatch and Williams' theory predicts a sharp edge at the lowest-left end of the multipactor region. In our simulation results, this section is rounded. Experimental data on this are scarce, but seem to validate our results [15].
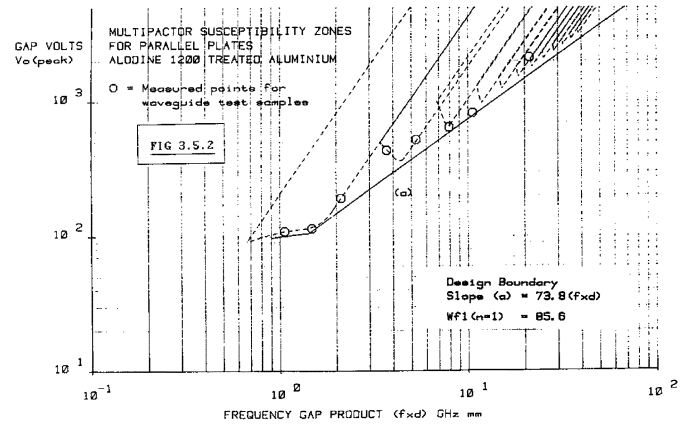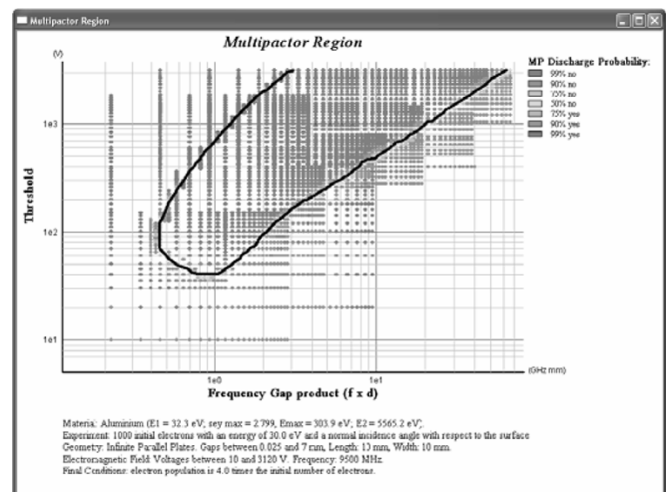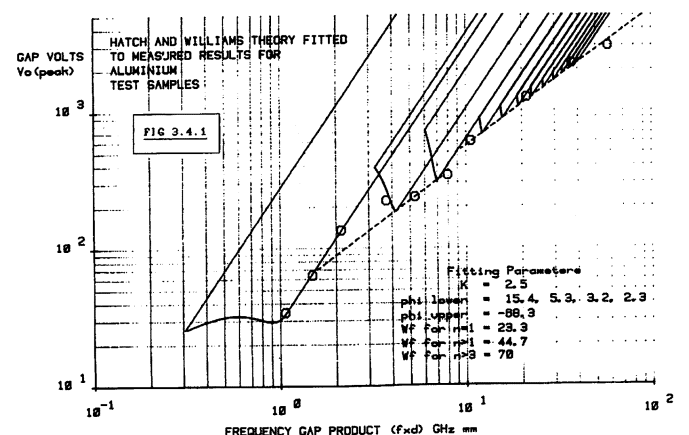
V. CONCLUSION AND FUTURE WORK

In this paper, we have described our MEST software tool for the prediction of the multipactor effect in parallel plates geometry. The software is based on a discrete-event model in which electrons are individually modeled and tracked. The application
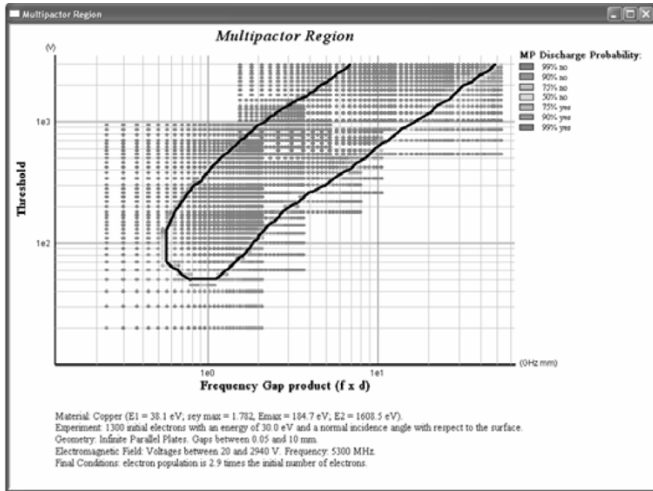
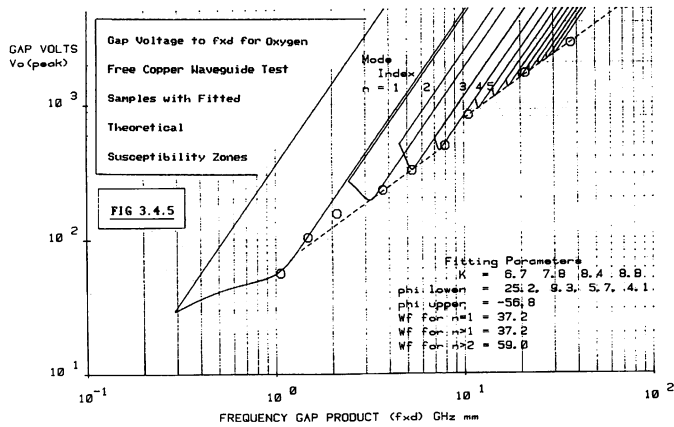Fig. 14. $V-f \cdot d$ region for Copper with MEST.

Fig. 15.   Experimental data for Copper from ESTEC, fitted with Hatch and Williams model, taken from [14].

provides a number of output forms that allows the visualization of the multipactor regions, and the evolution and positions of electrons during simulation. The results obtained show good agreement with available experimental results.

In the future, we will design a similar software for the prediction of the Corona effect [16]. Notice that for this effect the collisions of the electrons with the gas atoms have also to be considered.

REFERENCES

[1] P. T. Farnsworth, "Television by electron image scanning," *J. Franklin Inst.*, vol. 218, pp. 411–444, 1934.

[2] J. R. M. Vaugham, "Multipactor," *IEEE Trans. Electron Devices*, vol. 35, no. 7, pp. 1172–1180, Jul. 1988.

[3] G. Fishman, *Discrete Event Simulation. Modeling, Programming and Analysis*, ser. Springer Series in Operations Research.   New York: Springer-Verlag, 2001.

[4] G. Devaz, "Multipactor simulations in superconducting cavities and plasma couplers," *Phys. Rev.*, vol. 4, pp. 012 001–012 001, 2001.

[5] L. Galán, M. A. Jiménez, and F. Rueda, "Development of a Computer Model for the Multipactor Effect," ESA, ESA-ESTEC Contract 6577/85/NL/PB 1990/Rider, 1991.

[6] A. Valfell, R. A. Kishek, and Y. Y. Lau, "Frequency response of multipactor discharge," *Phys. Plamas.*, vol. 5, pp. 300–300, 1998.

[7] D. Vender, H. B. Smith, and R. W. Boswell, "Simulations of multipactor-assisted breakdown in radio frequency plasmas," *J. Apply. Phys.*, vol. 80, pp. 4292–4292, 1996.

[8] C. K. Birdsall, "Particle-in-Cell charged-particle simulations, plus monte carlo collisions with neutral atoms, PIC-MCC," *IEEE Trans. Plasma Sci.*, vol. 19, no. 2, Apr. 1991.

[9] R. Cimino, I. R. Collins, M. A. Furman, M. Pivi, F. Ruggiero, G. Rumolo, and F. Zimmermann, "Can low-enery electrons affect high-energy physics accelerators?," *Phys. Rev. Lett.*, vol. 93, pp. 014 801–014 801, 2004.

[10] L. Reimer, *Scanning Electron Microscopy. Physics of Image Formation and Microanalysis*, ser. Springer Series in Optical Sciences 45.   New York: Springer-Verlag, 1985, ch. 4.

[11] M. A. Furman and M. T. Pivi, "Probabilitic model for the simulation of secondary electron emission," *Phys. Rev.*, vol. 5, pp. 124 404–124 404, 2002.

[12] G. Booch, *Object Oriented Design*.   Boston, MA: Benjamin-Cummings, 1991.

[13] A. J. Hatch and H. B. Williams, "The secondary electron resonance of low-pressure high-frequency gas breakdown," *J. Appl. Phys.*, vol. 25, no. 4, Apr. 1954.

[14] A. Woode and J. E. Petit, "Diagnostic investigations into the multipactor effect, susceptibility zone measurements and parameters affecting a discharge," presented at the ESTEC, Noordwijk, The Netherlands, 1989, Working Paper 1556.

[15] R. Woo, "Final Report on RF Voltage Breakdown in Coaxial Transmission Lines,", NASA Rep. 32-1500.

[16] Y. P. Raizer, *Gas Discharge Physics*.   Berlin, Germany: Springer-Verlag, 1991.

Juan de Lara was born in Toledo, Spain, in January 1974. He received the B.S. degree in computer science from the University of Castilla la Mancha, Toledo, Spain, in 1994, and the M.S. and Ph.D. degrees from the Universidad Autónoma, Madrid, Spain, in 1996 and 2000, respectively.

He has been a postdoctoral researcher at McGill University, Montreal, QC, Canada, and Technical University of Berlin, Berlin, Germany. At present, he is an Associate Professor at the Computer Science Department of the Universidad Autónoma, where he teaches Modeling and Simulation and Software Engineering. He has published over 90 research papers in areas such as web-based simulation, agent-based simulation, object-oriented modeling, and simulation and multiparadigm modeling.

Francisco Pérez was born in Madrid, Spain, in 1979. He received the M.S. degree in computer science in 2001 from the Universidad Autónoma de Madrid, where he started working toward the Ph.D. degree in 2003.

His research interests include the design of domain-specific visual languages, component-based design, and the modelling and simulation of hybrid systems.

Manuel Alfonseca received the Ph.D. degree in electronics engineering and computer science from the Universidad Politecnica, Madrid, Spain, in 1972 and 1976, respectively.

He teaches and does research at the Department of Computer Science, Universidad Autonoma, Madrid, Spain, where he was Director of the Higher Polytechnical School (2001–2004). Previously, he was Senior Technical Staff Member at the IBM Madrid Scientific Center, Madrid, Spain, where he worked from 1972 to 1994. He has published over 200 papers and books on computer languages, simulation, complex systems, graphics, artificial intelligence, object-orientation, and theoretical computer science, as well as popular science and juvenile literature, with different awards in all of these fields.

He is a senior member of the Society for Modeling and Simulation International (SCS), the New York Academy of Sciences, the IEEE Computer Society, the Association for Computing Machinery (ACM), the British APL Association, the IBM Technical Experts Council, and the Spanish Association of Scientific Journalism.

Luis Galán received the Ph.D. degree in materials science and engineering from Stanford University, Stanford, CA, in 1980.

He is Tenure Professor (Profesor Titular) in the Department of Applied Physics, the Universidad Autónoma de Madrid, Madrid, Spain. He has published over 80 research papers. His present interest is in secondary emission properties of materials with application in space hardware, in relation with multipactor breakdown, including micro- and nano-structured surfaces. He has headed the research on this subject of the European Space Agency for many years. Other scientific interests include surface science, colour centres, photocathodes, carbon nitride, transition metals and compounds, XPS, UPS, AES, synchrotron radiation spectroscopic techniques, and ion beams techniques.

Isabel Montero received the Ph.D. degree in physics from Autónoma University of Madrid, Madrid, Spain, in 1984.

She is currently a Senior Scientist with the Materials Science Institute of Madrid of the Spanish National Research Council (CSIC), Madrid, Spain. She has used a wide array of spectroscopy techniques including X-ray photoelectron spectroscopy (XPS), Auger spectroscopy (AES), secondary and backscattered electron spectroscopy, and electron stimulated desorption (ESD). She has published over 100 papers on materials science and applied physics. Her recent work with photoemission spectroscopy using synchrotron radiation has focused on resonance phenomenon. Her research interests revolve on multipactor discharge and algorithms. Another active area of her research is the measurements of secondary electron emission yields of insulator materials; this has application to understanding the charging of spacecraft in near-earth orbit.

Elisa Román received the Ph.D. degree in physics from Autonoma University, Madrid, Spain, in 1977.

She is currently a Senior Scientist of the staff of the Materials Science Institute of Madrid. She was appointed to National Research Council and the British Royal Society Postdoctoral Fellowship at the Department of Electrical Engineering and Electronics University of Liverpool, Liverpool, U.K. She was at the U.S. National Bureau of Standards, as Visitor Scientist, as well as at the Interdisciplinary Research Center in Surface Science, University of Liverpool. Her scientific interest are in the area of gas/liquid-surface interactions in order to improve the catalytic activity of metals, semiconductors and oxide surfaces as well as low friction coating (LFC) and environmental adapted lubricants (EAL) in order to improve their tribological properties. She is expertise in UHV Technique. She is an specialist with a high experience and background in XPS, UPS, and synchrotron radiation techniques applied to the study of nanostructures, surface science and material engineering. She has published more than 80 refereed papers.

David Raboso Garcia-Baquero was born in Alcazar De San Juan, Spain, in 1967. He studied at Instituto Cervantes, Madrid, Spain, and received the M.S. degree in physics from the University Autonoma, Madrid, Spain.

In 1992, he was detached to The Netherlands to work at ESTEC, the main Research Center of the European Space Agency (ESA). Since then, he has been deeply involved in all European space programs where RF breakdown was considered a potential threat to the success of the mission. He is the contact point of all research activities at ESA in the field of multipactor, corona, and passive intermodulation including the organization of the only international workshop dedicated to these issues, MULCOPIM.